Available online at www.sciencedirect.com
SCIENCE DIRECT®
International Journal of Heat and Mass Transfer 48 (2005) 4510–4517
International Journal of HEAT and MASS TRANSFER
www.elsevier.com/locate/ijhmt

Mass transport and fluid flow in stenotic arteries: Axisymmetric and asymmetric models

M.R. Kaazempur-Mofrad [a,1], S. Wada [b,1], J.G. Myers [a,2], C.R. Ethier [a,c,*]

[a] Department of Mechanical and Industrial Engineering, University of Toronto, Toronto, Ont., Canada M5S 3G8
[b] Department of Bioengineering and Robotics, Tohoku University, Sendai, Japan
[c] Institute for Biomaterial and Biomedical Engineering, University of Toronto, Toronto, Ont., Canada M5S 3G8

Received 7 October 2004; received in revised form 22 March 2005

Abstract

Mass transport may play a significant role in the development of atherosclerosis, a progressive disease of the artery wall. In this work, advection-dominated transport of blood-borne components such as oxygen and ATP is considered in two arterial models with mild (56% area reduction) stenoses, representative of the early stages of disease development. Flow and mass transport patterns in a symmetric stenosis are contrasted with those in an asymmetric model. The complex flow field due to the asymmetric stenosis (which is a more realistic representation of the diseased arteries) resulted in mass transfer patterns substantially different than those exhibited by the axisymmetric stenosis. This implies that accurate representation of arterial geometries is essential when the link between mass transfer and atherosclerosis is sought.

Keywords: Fluid flow; Mass transfer; Atherosclerosis; Stenosis; Axisymmetric; Asymmetric; Finite element method

1. Introduction

Atherosclerosis is the leading cause of morbidity and mortality in Western societies. It is a progressive disease characterized by localized plaques that form within the artery wall. As the disease progresses, these plaques enlarge and, either directly or indirectly, lead to impairment of blood flow. This in turn can have serious consequences, such as blockage of the coronary arteries (leading to myocardial infarction) and carotid arteries (leading to strokes as plaques detach and occlude the cerebral vasculature). Atherosclerotic lesions are found preferentially at specific sites in the arterial system, typically near bifurcations, bends, and other regions characterized by "complex" blood flow patterns [1].

These observations, as well as data about the response of endothelial cells to mechanical forces, suggest that hemodynamics, i.e. fluid dynamic related phenomena, play a role in the initiation and progression of atherosclerosis. In particular, low and oscillatory wall shear stress (WSS) has been found to be positively correlated to localized intimal thickening of the arterial wall

* Corresponding author. Address: Department of Mechanical and Industrial Engineering, University of Toronto, 5 King's College Road, Toronto, Ont., Canada M5S 3G8. Tel./fax: +416 978 6728/7753.
E-mail address: ethier@mie.utoronto.ca (C.R. Ethier).
[1] Both authors contributed equally to this work.
[2] Current affiliation: NASA-Glenn Research Center.

0017-9310/$ - see front matter © 2005 Elsevier Ltd. All rights reserved.
doi:10.1016/j.ijheatmasstransfer.2005.05.004

[2–5]. However, the relationship between WSS and arterial disease is far from being well-understood [6]. WSS plays an important role in remodelling the arterial wall [7] and can lead to arterial wall thickening (intimal hyperplasia), but hyperplastic regions of the artery wall do not invariably progress to develop atherosclerotic disease. Moreover, the correlation between WSS and intimal thickening is unconvincing in some arteries [8,9]. Taken together, these data suggest that WSS may not be the only mechanism that promotes atherogenesis (the initiation of atherosclerotic lesions). Caro et al. [10] suggested that atherosclerosis may occur due to a shear dependent mass transfer mechanism. Further, hypoxia associated with low oxygen transfer has been linked to initiation of atherosclerosis (see [11] and references therein). In order to assess the possible correlation between sites of atherosclerotic disease and mass transport patterns, accurate characterization of local mass transport features is required.

The goal of this paper is to study mass transfer in two idealized arterial models with mild (56% cross-sectional area reduction) stenosis. Quantitative assessment of flow and mass transfer in mild stenoses is of great importance, since such stenoses represent the early stage of disease development. Several studies have examined fluid flow and mass transfer patterns in axisymmetric stenoses, but there are only a few studies in asymmetric stenoses. For example, Ojha et al. [12] and Yamaguchi and Hanai [13,14] studied flow in asymmetric stenoses, showing that asymmetry markedly affected flow and wall shear stress patterns. Wada et al. [15] modelled flow and low density lipoprotein mass transport in an arterial junction that included an asymmetric stenosis, showing asymmetric mass transfer patterns.

Because real atherosclerotic lesions are asymmetric, we need to better understand factors controlling mass transfer in such geometries. This has prompted us to investigate the effect of the asymmetry on fluid flow and mass transport patterns in stenoses. A Schmidt number of $Sc = 3000$ suitable for oxygen and ATP is assumed.

2. Methods

2.1. Stenosis geometries

The axisymmetric and asymmetric (off-centered) 56% area reduction stenoses used in this work are shown in Fig. 1. The total length of each model was $20D$, aligned along the z-axis, where D is the diameter of the non-stenosed part of the artery. The length of the stenosis in both models was $4D$, with the center of the stenosis positioned at $z = 0$, leaving $14D$ downstream of the stenosis for the flow to redevelop, and $2D$ upstream of the stenosis as an entrance length.

The axisymmetric stenosis had the following cosine shape:

$$\frac{r}{R} = 1 - \frac{\delta}{D}\left(1 + \cos\left(\frac{2\pi z}{Z_0}\right)\right) \tag{1}$$

for $-2D < z < 2D$, where $r = r(z)$ is the radius of the artery at location z in the stenosed region, R is the radius of the non-stenosed part of the artery, δ is the maximum

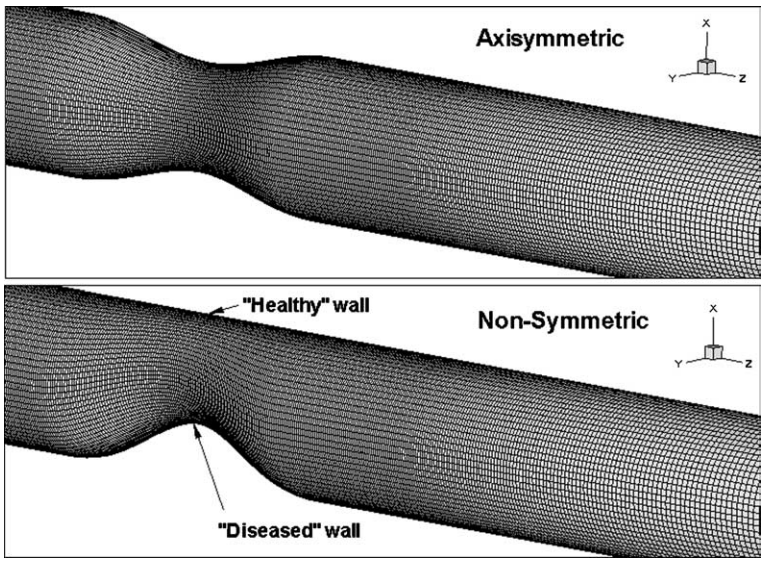

Fig. 1. Views of the stenosis regions in the two models, with mass transfer surface meshes overlain. Note that the z-axis has been foreshortened by a factor of two.

radius reduction at the throat of the stenosis ($D/6$), and Z_0 is the length of the stenosis ($4D$). The asymmetric stenosis model was made by using the same circular cross-sections as defined by Eq. (1), with the centre of each cross-section being offset in the x direction by an amount $D - r$. This resulted in a smooth, eccentric stenosis with a "healthy" wall (no profile change) and a "diseased" wall (Fig. 1).

2.2. Modeling conditions and numerical details

Steady flow and mass transfer were considered in arteries with rigid and stationary walls. Although it is believed that physiological unsteadiness significantly affects both flow field and mass transfer patterns, the steady state assumption is reasonable for the initial stages of this study. Blood was assumed to have Newtonian rheology. The non-Newtonian viscosity of blood has been found to have little effect in the dynamics of blood flow in the large arteries of interest [16,17].

The Reynolds number was $Re_D = VD/\nu = 250$, where V is mean inlet velocity, D is inlet diameter and ν is blood kinematic viscosity. The Schmidt number was $Sc = \nu/\mathscr{D} = 3000$, where $\mathscr{D}$ is the diffusivity of the transported species in blood. This value is representative of relatively small species such as ATP or free oxygen in blood. In the case of oxygen, which is carried both dissolved in plasma and bound to hemoglobin in red cells, the effective diffusivity is a non-linear function of local oxygen concentration [18], which we did not account for in this study. Although the inclusion of oxygen bound to hemoglobin somewhat modifies the details of the mass transfer process we chose to focus on free oxygen transport, given that the primary objective of the present work is to address the importance of accurate geometrical representation in physiological mass transfer calculations. The flow boundary conditions were as follows: a fully developed velocity profile was imposed at the inlet, the no-slip velocity boundary condition was set on the walls, and the traction-free boundary condition was applied at the outlet. The mass transfer boundary conditions were as follows: a uniform dimensionless concentration of $c = 1$ was imposed at the inlet, a Dirichlet boundary condition of $c = 0$ was set on the walls, and a zero gradient in c was applied at the outlet. Setting $c = 0$ on the artery wall essentially neglects coupling between mass transport in the blood and in the artery wall, and is appropriate, for example, when the fluid-side mass transport resistance dominates the wall-side resistance, as discussed in greater detail in [19].

The key outcome measure in these simulations was the mass flux to the arterial wall, quantified through the Sherwood number, $Sh_D = nD/(\mathscr{D}\Delta c)$, where n is the local mass flux to the artery wall and Δc is a reference concentration difference, in this case the inlet concentration minus the wall concentration. The mass flux n was computed by numerical differentiation of the concentration gradient at the wall.

Use was made of the existence of a symmetry plane and only half of the geometry was considered in both artery models. The mesh used for modeling the flow in both stenosis models had 360,640 linear brick elements (380,817 nodes). In the circumferential direction, 40 elements were used for the half-geometry, while in the z-direction, the mesh spacing was $D/30$ for $-4 < z/D < 4$, and then gradually increased towards $0.15126D$ at the outlet. In the non-stenosed region, the element size in the radial direction was $0.02D$ at the center of the vessel and $0.00565D$ at the circumference, with proportional reductions in the stenosed region of the vessel.

To model the mass transfer field, the four layers of elements near the wall were subdivided to give meshes with 517,440 linear brick elements (541,947 nodes). The subdivision was non-uniform, with the outermost layer of flow elements being radially subdivided into five layers of mass transfer elements, the next layer of flow elements being subdivided into four layers of mass transfer elements, etc. The resulting off-wall spacing was $D/885$ in the non-stenosed region of the artery, with proportional reduction in off-wall spacing in the stenosis region.

The 3-D, steady, incompressible Navier–Stokes equations were solved with a commercial finite volume package (STAR-LT 2003 SR-1). Default settings were used, namely: the steady flow option, the SIMPLE formulation, first order upwind differencing for velocity and central differencing for pressure on a staggered grid. Convergence was achieved when the maximum mass and momentum residuals fell below 10^{-4}. For the mass transfer calculations the 3-D steady advection-diffusion equation was solved with a validated finite element code based on the streamline upwind Petrov–Galerkin method [15,20,21] using linear hexahedral 8-noded finite elements.

3. Results

3.1. Axisymmetric stenosis model

Flow accelerates in the converging part of the axisymmetric stenosis and a high momentum jet is formed at the throat (Fig. 2). The velocity profile then expands gradually and smoothly downstream of the stenosis. The flow in the axisymmetric stenosis model experiences a small and weak recirculation zone, as denoted by the black bar in Fig. 2. No circumferential asymmetries occur, as expected. The thickness of the momentum boundary layer slightly increases as a result of the expansion distal to the throat of the stenosis constriction, which extends to about $8D$ downstream of the throat.

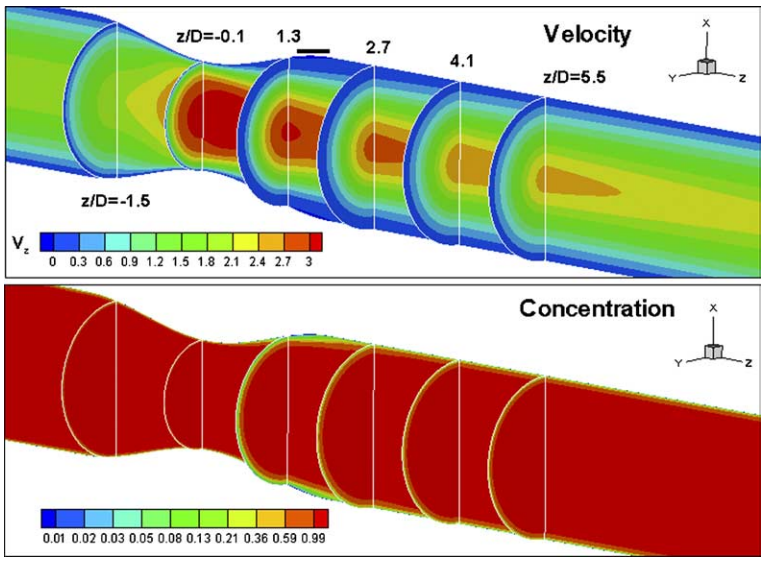

Fig. 2. Velocity and concentration profiles in the axisymmetric stenosis model. Upper panel: a contour plot of normalized axial velocity (V_z) on the centre plane of the stenosis and selected cross-sectional slices. The small bar on the upper edge shows the extent of the (weak) separation zone; the corresponding bar on the lower edge is not shown for clarity. The axial velocity has been normalized by the mean inlet velocity. Lower panel: corresponding normalized concentration contours, plotted using a non-linear scale bar. Note that the z-axis has been foreshortened by a factor of two in both panels.

The concentration patterns follow the flow field as expected. As we approach the throat of the stenosis, the concentration boundary layer thins towards a minimum at the throat (Fig. 2). Downstream of the stenosis throat the concentration boundary layer thickens as the low velocity region of flow, including the weak recirculation zone, allows the mass transfer boundary layer to grow. This trend continues until approximately $z/D = 1$ where the concentration boundary layer experiences its maximum thickness. The concentration boundary layer thickness starts to decrease again as the low velocity region becomes smaller. The concentration pattern is symmetric over the arterial cross-sections.

For a more quantitative insight into flow and mass transport patterns in the axisymmetric stenosis, the normalized wall shear stress and Sherwood number (Sh_D) were next examined (see Fig. 3). The shear stress peaks just proximal to the stenosis throat and shows the weak recirculation zone between $z/D = 1.5$ and 2. The Sh_D distribution at the inlet section agrees very well with the Graetz–Nusselt solution, indicating that the computational mesh used was sufficient to resolve relevant flow and mass transfer features. The maximum mass transfer rate occurs slightly upstream of the stenosis throat, similar to the WSS peak. The minimum value of Sh_D is nearly zero, and occurs at $z/D = 1.5$, i.e. in the low velocity region downstream of the throat. The Sherwood number then starts to increase as the mass transfer boundary layer thins due to a reduction in the size of the low momentum flow region, asymptoting to the distribution expected for a non-stenosed artery (Graetz–Nusselt solution).

3.2. Asymmetric stenosis model

The flow field in the asymmetric stenosis model is much more complex than in the axisymmetric model. Similar to the axisymmetric stenosis, the flow accelerates in the converging part of the asymmetric stenosis (Fig. 4). However, the non-symmetric contraction leads to a secondary flow directed primarily towards the healthy wall (see cross-sectional contour at $z/D = -1.5$). As the flow nears the throat, the axial flow streamlines curve to follow the contour of the diseased wall, inducing a transverse pressure gradient and a corresponding secondary flow. This produces a weak Dean-like vortex that is superimposed on the upstream contraction flow (see cross-sectional contour at $z/D = -0.1$). Distal to the throat there is a prominent and complex retrograde flow zone on the diseased wall, which extends along the symmetry plane for about three diameters downstream of the throat. The three-dimensional nature of this retrograde flow zone can be partially appreciated from the cross-sectional slices at $z/D = 1.3$ and 2.7 in Fig. 4, which shows how the distal portion of this zone is "fed" with fluid from above. A complex interaction between the retrograde flow zone and the expansion of the high-momentum fluid core distal to the throat causes a reversal of the secondary flow circulation patterns at $z/D = 1.3$. Vorticity generated near the throat causes a stream-wise

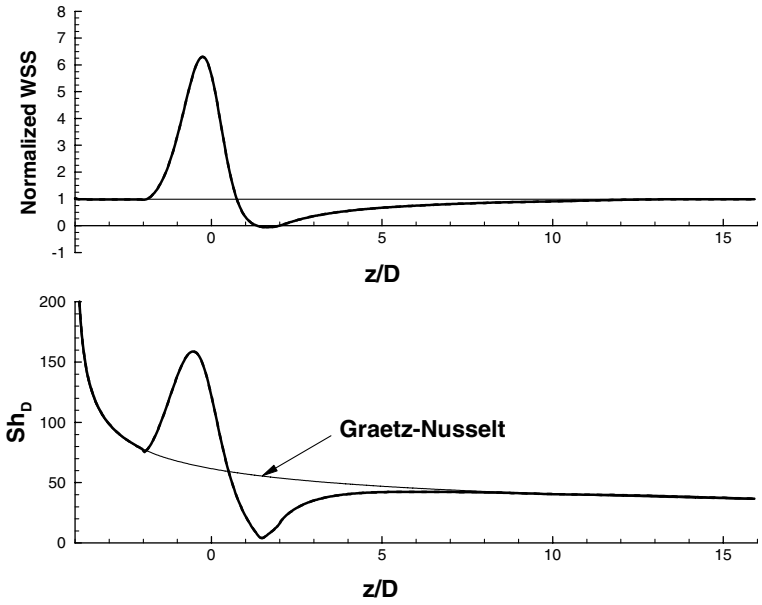

Fig. 3. Distribution of normalized WSS (top panel) and Sh_D (bottom panel) in the axisymmetric stenosis with 56% area reduction. Wall shear stress is normalized by the Poiseuille value in a non-stenosed tube (thin line). The Sherwood number predicted by the Levesque solution (high Schmidt number form of the Graetz–Nusselt solution [22]) is shown in the bottom panel for reference.

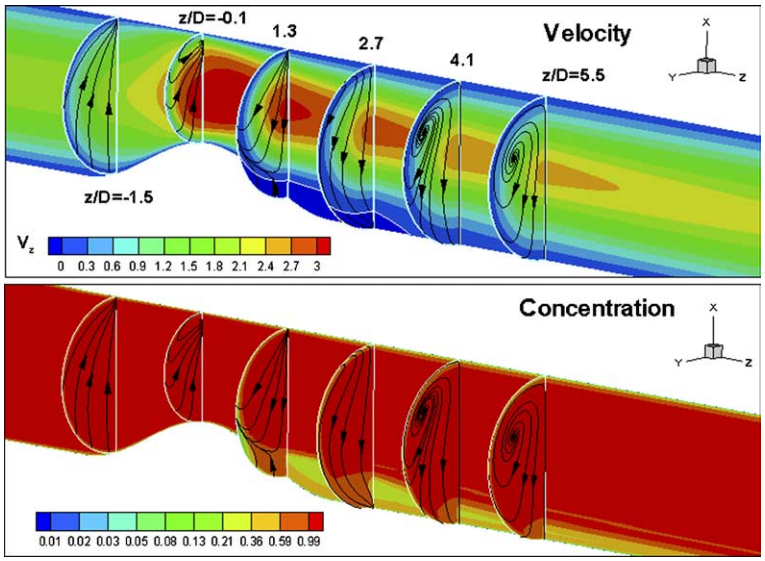

Fig. 4. Velocity and concentration profiles in the non-symmetric stenosis model. Plot is similar to Fig. 2 except that secondary flow streamlines have been shown on cross-sections, and the contour of zero axial velocity (V_z) has been highlighted in white in the upper panel so as to better identify the retrograde flow zone.

vortex to form, which becomes evident for $z/D > 3$, and eventually dissipates much further downstream.

The corresponding concentration profiles are shown in the lower panel of Fig. 4, and are dominated by the interaction between the retrograde flow zone and the secondary flows. For example, there is an extensive region of low concentration fluid on the symmetry plane. This fluid flows retrograde and then splits into two main streams. One stream flows circumferentially along the side wall towards the healthy side of the artery, creating

a crescent of low-concentration fluid that extends up the side walls of the stenosis just distal to the throat. The other stream stays close to the symmetry plane and leaves the "top" of the retrograde flow zone, moving slowly downstream and creating a "tail" of low-concentration fluid that extends for a great distance along the diseased wall.

More insight into the separation distal to the stenosis throat can be obtained from looking at the so-called "limiting streamline" field (also called "wall streamlines" or "skin friction lines"; see [23]). The limiting streamlines are interpreted as trajectories arising from the vector-valued wall shear stress field on the solid surface, and are shown for the case of the asymmetric stenosis in Fig. 5. In that figure we have also identified the singular points in the limiting streamline field, which are points where both components of the shear stress vanish. Such points can be classified as saddle points or nodes, and must obey a constraint on their distribution arising from kinematics [23,24]. Separation is not trivial to define in three dimensions, and occurs when limiting streamlines converge onto one particular limiting streamline emanating from a saddle point [23,25]. The limiting streamline onto which multiple streamlines converge is the line of separation. Fig. 5 shows that a line of separation emanates from the separation point on the symmetry plane, runs along the side wall, and terminates at the focus. There is also a line of attachment running along the side wall that passes through a saddle point on the symmetry plane.

The Sherwood number distribution in the asymmetric stenosis is quite complex, and reflects the strong secondary flows present in this geometry. The maximum Sherwood number occurs on the symmetry plane slightly proximal to the stenosis throat, at $z/D \sim -0.5$. Distal to the stenosis, the Sherwood number is low in a broad zone on the side wall along the line of separation and around the focus point. The minimum value of the Sherwood number for the entire domain is approximately 1.2, which occurs by the focus point. The Sherwood number is slightly elevated in the reattachment region on the diseased wall and along the side wall, particularly distal to the reattachment point.

Further insight into mass transfer is obtained by examining wall shear stress and Sherwood number distributions (Fig. 6). Along the diseased wall, the lowest mass transfer rate is experienced at the separation point, where the Sherwood number is only about 5% of its peak value. There is a small local maximum in the Sh_D distribution curve on the diseased wall at $z/D \sim 1.5$, corresponding to the re-attachment point. However, other than this local effect, the Sherwood number distal to the throat is lower than that for a non-stenosed artery (Graetz–Nusselt solution) for an extended length along the diseased wall. This can be understood in the context of the extended low concentration "tail" described above. The minimum in Sherwood number at the focus is also clearly visible in this figure. There is also a modest thickening of the mass transfer bounder layer and corresponding reduction in the Sherwood number downstream of the stenosis on the healthy wall.

When comparing the axisymmetric and asymmetric stenoses, it is remarkable how different the velocity and concentration profiles are. This of course leads to corresponding differences in the wall shear stress, but most importantly in the Sherwood number distribution (compare Figs. 3 and 6). For example, even though the peak wall shear stress differs by about 20% between the healthy and diseased walls, the corresponding Sherwood number difference is about 40%. Generally speaking, the advection-dominated mass transport seen in this problem is more strongly affected by the secondary flows

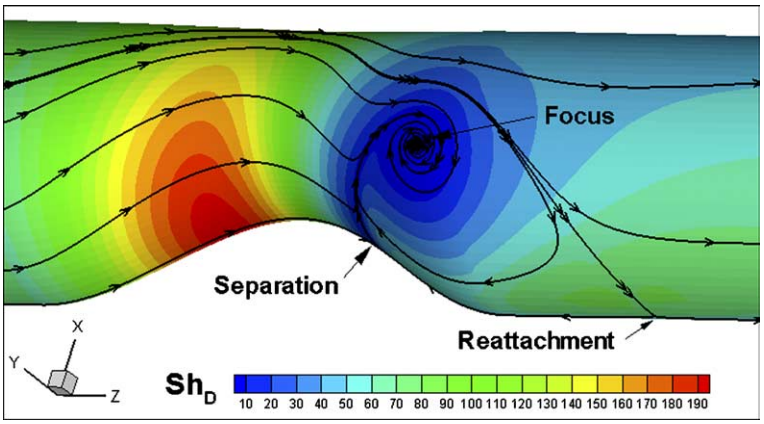

Fig. 5. Limiting streamline and counters of Sherwood number, Sh_D, in the non-symmetric stenosis model. In total there are four singular points in the limiting streamline distribution: two saddle points labeled "Separation" and "Reattachment" and two symmetric nodal points labeled "Focus", only one of which is visible in this view. This is a perspective (3-D) view of the side wall of the stenosis, turned slightly so that the axis of symmetry is at the lower edge of the figure. See text for definition of limiting streamlines.

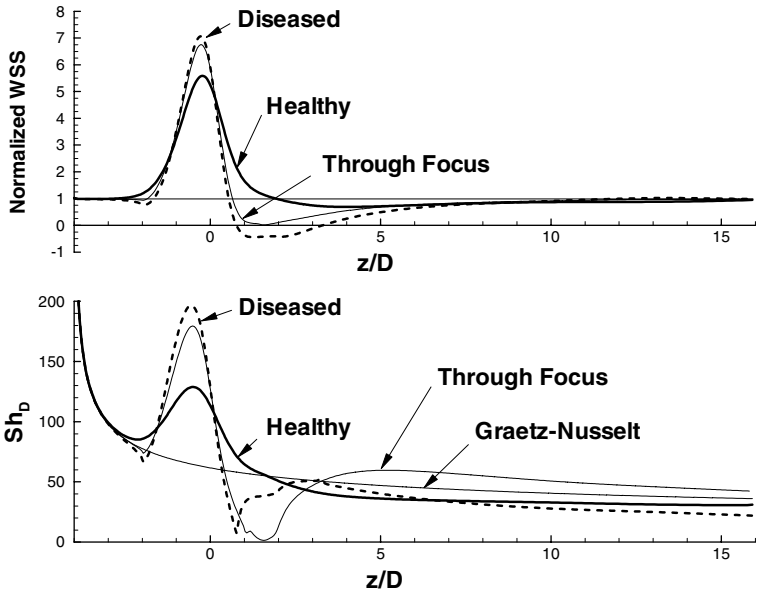

Fig. 6. Distribution of normalized WSS (top panel) and Sh_D (bottom panel) in the asymmetric stenosis with 56% area reduction. "Through Focus" refers to data extracted from a line of constant $\theta = \tan^{-1}(x/y)$ passing through the focus; "Diseased" and "Healthy" refer to data extracted along the bottom and top walls on the symmetry plane, corresponding to $\theta = -90°$ and $+90°$, respectively. Here wall shear stress refers to total wall shear stress magnitude. See Fig. 3 for further details of plot.

than is the momentum transport. That is, due to low diffusion coefficients, geometric effects have a more prolonged effect on mass transfer patterns than on flow patterns.

4. Summary and conclusions

Flow and mass transfer patterns were simulated in two arterial stenosis models with 56% area reduction representing the early to middle stages of atherosclerotic disease development. Axisymmetric and asymmetric cases were examined. The detailed geometry of in vivo stenoses is rarely known. However, as this study shows, the flow and mass transfer patterns are strongly dependent on the shape of the stenosis.

Similarities exist between the two models, as both show a tendency of the mass transfer boundary layer to thicken downstream of the stenosis. However, the two models differ in their mass transfer patterns in the immediate neighbourhood and distal to the stenosis. In the asymmetric stenosis model, which is a more realistic representation of diseased arteries, the development of downstream secondary flow features contributed to circumferentially non-uniform concentration distributions and to mass transfer patterns that are different than those in idealized axisymmetric stenoses. Higher Reynolds numbers and higher area reductions would be expected to enhance the significance of these secondary features. This underlines the importance of accurate representation of arterial geometries when the link between mass transfer and atherosclerosis is sought.

A limitation of this work is that only steady flow and mass transfer have been considered. The effects of unsteadiness in arterial mass transfer have been discussed in [19]; for high Schmidt numbers, there are not large differences between the steady case and the time-averaged unsteady case. However, this assumes that there are no instabilities in the flow, which for flow through a stenosis can occur for certain ranges of Reynolds number and stenosis severity [12]. A second limitation is that we have considered only half of the computational domain, thereby excluding any symmetry-breaking flow features which can be triggered by very small perturbations [26]. For physiologically-shaped stenoses (which are never symmetric) this is less of an issue.

Acknowledgements

This work was supported by the Natural Sciences and Engineering Research Council (CRE), the Canada Research Chairs Program (CRE) and a Grant-in-Aid for the 21st Century COE "Future Medical Engineering based on Bio-nanotechnology" from the Ministry of Education, Culture, Sports, Science and Technology of Japan (SW).

References

[1] D.M. Wootton, D.N. Ku, Fluid mechanics of vascular systems, diseases, and thrombosis, Annu. Rev. Biomed. Eng. 1 (1999) 299–329.

[2] D.N. Ku, D.P. Giddens, C.K. Zarins, S. Glagov, Pulsatile flow and atherosclerosis in the human carotid bifurcation: positive correlation between plaque location and low and oscillating shear stress, Arteriosclerosis 5 (1985) 293–302.

[3] M.H. Friedman, G.M. Hutchins, C.B. Bargeron, O.J. Deters, F.F. Mark, Correlation between intimal thickness and fluid shear in human arteries, Atherosclerosis 39 (1981) 425–436.

[4] X. He, D.N. Ku, Pulsatile flow in the human left coronary artery bifurcation: average conditions, ASME J. Biomech. Eng. 118 (1996) 74–82.

[5] M. Bonert, R.L. Leask, J. Butany, C.R. Ethier, J.G. Myers, K.W. Johnston, M. Ojha, The relationship between wall shear stress distributions and intimal thickening in the human abdominal aorta, Biomed. Eng. Online 2 (2003) 18.

[6] M.R. Kaazempur-Mofrad, A.G. Isasi, H.F. Younis, R.C. Chan, D.P. Hinton, G. Sukhova, G.M. LaMuraglia, R.T. Lee, R.D. Kamm, Characterization of the atherosclerotic carotid bifurcation using MRI, finite element modeling, and histology, Ann. Biomed. Eng. 32 (2004) 932–946.

[7] B.L. Langille, F. O'Donnell, Reductions in arterial diameter produced by chronic decreases in blood flow are endothelium-dependent, Science 231 (1986) 405–407.

[8] A.K. Joshi, R.L. Leask, J.G. Myers, M. Ojha, J. Butany, C.R. Ethier, Intimal thickness is not associated with wall shear stress patterns in the human right coronary artery, Arteriosclerosis Thromb. Vasc. Biol. 24 (2004) 2408–2413.

[9] D.A. Steinman, J.B. Thomas, H.M. Ladak, J.S. Milner, B.K. Rutt, J.D. Spence, Reconstruction of carotid bifurcation hemodynamics and wall thickness using computational fluid dynamics and MRI, Magn. Reson. Med. 47 (2002) 149–159.

[10] C.G. Caro, J.M. Fitz-Gerald, R.C. Schroter, Atheroma and arterial wall shear. Observation, correlation and proposal of a shear dependent mass transfer mechanism for atherogenesis, Proc. Roy. Soc. Lond. B Biol. Sci. 177 (1971) 109–159.

[11] G. Schneiderman, C.G. Ellis, T.K. Goldstick, Mass transport to walls of stenosed arteries: variation with Reynolds number and blood flow separation, J. Biomech. 12 (1979) 869–877.

[12] M. Ojha, R.S.C. Cobbold, K.W. Johnston, R.L. Hummel, Pulsatile flow through constricted tubes: an experimental investigation using photochromic tracer methods, J. Fluid Mech. 203 (1989) 173–197.

[13] T. Yamaguchi, S. Hanai, To what extent does a minimal atherosclerotic plaque alter the arterial wall shear stress distribution? A model study by an electrochemical method, Biorheology 25 (1988) 31–36.

[14] T. Yamaguchi, S. Hanai, Measured wall shear stress distribution pattern upstream and downstream of a unilateral stenosis by an electrochemical method, Biorheology 24 (1987) 753–762.

[15] S. Wada, M. Koujiya, T. Karino, Theoretical study of the effect of local flow disturbances on the concentration of low-density lipoproteins at the luminal surface of end-to-end anastomosed vessels, Med. Biol. Eng Comput. 40 (2002) 576–587.

[16] P.D. Ballyk, D.A. Steinman, C.R. Ethier, Simulation of non-Newtonian blood flow in an end-to-side anastomosis, Biorheology 31 (1994) 565–586.

[17] K. Perktold, R.O. Peter, M. Resch, G. Langs, Pulsatile non-Newtonian blood flow in three-dimensional carotid bifurcation models: a numerical study of flow phenomena under different bifurcation angles, J. Biomed. Eng. 13 (1991) 507–515.

[18] J.A. Moore, C.R. Ethier, Oxygen mass transfer calculations in large arteries, J. Biomech. Eng. 119 (1997) 469–475.

[19] C.R. Ethier, Computational modeling of mass transfer and links to atherosclerosis, Ann. Biomed. Eng. 30 (2002) 461–471.

[20] S. Wada, T. Karino, Theoretical prediction of low-density lipoproteins concentration at the luminal surface of an artery with a multiple bend, Ann. Biomed. Eng. 30 (2002) 778–791.

[21] S. Wada, T. Karino, Prediction of LDL concentration at the luminal surface of a vascular endothelium, Biorheology 39 (2002) 331–336.

[22] R.B. Bird, W.E. Stewart, E.N. Lightfoot, Transport Phenomena, John Wiley & Sons, New York, 1960.

[23] M. Tobak, D.J. Peake, Topology of three-dimensional separated flows, Ann. Rev. Fluid Mech. 14 (1982) 61–85.

[24] J.C. Hunt, C.J. Abell, J.A. Peterka, H. Woo, Kinematical studies of the flows around free or surface-mounted obstacles; applying topology to flow visualization, J. Fluid Mech. 86 (1978) 179–200.

[25] C.R. Ethier, S. Prakash, D.A. Steinman, R.L. Leask, G.G. Couch, M. Ojha, Steady flow separation patterns in a 45 degree junction, J. Fluid Mech. 411 (2000) 1–38.

[26] M. Fearn, T. Mullin, K.A. Cliffe, Nonlinear flow phenomenon in a symmetric sudden expansion, J. Fluid Mech. 211 (1990) 595–608.